TEMPERATURE-BASED ESTIMATION OF EPICYCLIC GEARBOX DISSIPATION

Levi Gershon
Massachusetts Institute of Technology
Cambridge, MA, Untied States of America

ABSTRACT

Gearbox thermal dissipation is a key performance parameter for gearboxes' safe design and operation. However, dissipation varies with respect to operating load and speed, and is complex to predict a priori. To characterize the performance of MIT Motorsport's planetary gearbox, temperature measurements were used together with a thermal network model to estimate the total steady-state dissipated power, P_{disp}, at various operating speeds. A polynomial proportional function was fitted to the resulting data, yielding a power dependence of $P(\omega) \propto \omega^{5/3}$, where ω is the operating speed in RPM. Per industry standards, the $\omega^{5/3}$ dependence indicates that lubricant churning effects likely dominate heat generation, and hence suggests that future work should focus on the lubrication dynamics [1].

Keywords: Epicyclic, gearbox, thermal network, dissipation, speed

1. INTRODUCTION

Planetary gearboxes – also called epicyclic gearboxes, constituting a solar-system like arrangement of concentrically rotating gears – are used in numerous safety-critical applications, from wind turbines to electric vehicles [2, 3]. Their efficiency is a key performance parameter, affecting both the power delivered to the load, and the cooling hardware needed to run the gearbox. In an electric vehicle, for instance, the battery size must be increased if the gearbox is less efficient, and a cooling system potentially added to dissipate the heat generated by that inefficiency. Alternatively, for wind turbines, the added thermal dissipation of inefficiency will again require investment in cooling systems, and constitute lost revenue in potential electricity generation. Furthermore, since planetary gearboxes are often assembled using interference fits, which can fail at high temperatures due to differential thermal expansion, determining gearbox inefficiency is paramount to safe and reliable operation [4].

Predicting gearbox dissipation, however, is a difficult endeavor. High contact pressures between the gears, as well as the presence of the lubrication film create a complex viscoelastic loading scenario [5]. Both Sivayogan *et al.* and Wang *et al.* have created extensive non-linear models of gear contact behavior, and then used thermal network modeling to transform the gear contact dynamics into temperature rises in the bulk gear material [5, 6]. The gears are only one element of a gearbox, however, and the overall thermal behavior must also include heat from the bearings. In a recent paper, Neurouth et al, developed a thermal network model of rolling element bearing dissipation, and validated it against experimental data [7].

Combining these sources of dissipation – the viscous dissipation from the gear contact dynamics, as well as the rolling element bearing losses – to find the efficiency of a gearbox is a complex modeling problem. Additionally, that inefficiency may not be constant with respect to operating speed and load. For instance, using a dynamometer, Břoušek *et al.* measured the efficiency of a gearbox at varying speeds and applied torques, and found that at a constant load of 20 Nm, the efficiency dropped from 96% to 92% between 750 and 3000 RPM (revolutions per minute) [8]. Their work was experimental in nature, however, without the ability to generalize to other system geometries. Here too, with holistic gearbox analysis, thermal network modeling has been used to integrate component-level dynamics into larger models. Complete models of gearbox dissipation have been created that combine gear friction, rolling element bearing friction, and viscous losses into large thermal networks, but they result in heavily parametrized models, ill-suited for rapid design iteration [9–12].

Due to these complexities, to better facilitate planetary gearbox design this project aimed to measure the thermal dissipation of an example gearbox as a function of the rotational speed, using simple thermal techniques. A case study was conducted on a single-stage planetary gearbox designed by MIT Motorsports, a test apparatus

constructed, and the temperature monitored via thermocouples. A thermal network model of the gearbox was derived and then calibrated based on temperature decay of the gearbox from a known value to ambient. Next, the steady state temperature and time-domain parameters of the gearbox housing and ring gear were measured over a sweep of operating speeds from 1000 RPM to 7000 RPM. The resulting dissipated power estimates are found to fit a $\omega^{5/3}$ dependence, implying that gear lubricant churning losses dominate heat generation, and hence that future design should focus on minimizing lubrication losses. This generated data will in turn aid gearbox hardware engineers, both specifically on MIT Motorsports and in general in making products safer, faster to design, and more efficient.

2. BACKGROUND

2.1 PLANETARY GEARBOXES

To achieve compact, high power density transmission, epicyclic gear trains are sometimes used. Also known as planetary gear trains, their names derive from the concentric axes of rotation of several rotating elements, akin to a solar system model. Instead of conventional spur-gear architectures, where the axes of rotation are held fixed, planetary gearboxes permit the axes of some of the gears to rotate in turn, as seen in Figure 1. A sun gear in the center rotates several planet gears, which in turn rotate an internal ring gear. This does not change the overall system dynamics, however: conservation of power still guarantees the relationship in Equation (1), for some nominal efficiency η, input speed ω_{in}, input torque τ_{in}, and power delivered to load P_{out}.

$$P_{out} = \eta \omega_{in} \tau_{in} \tag{1}$$

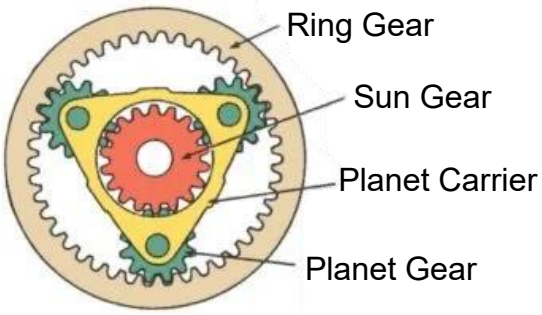

Figure 1: A schematic of a typical single-stage planetary gear train. The sun gear is located in the center, as the canonical sun of a solar system, with the three planet gears orbiting it as the planet carrier rotates about the central axis. An internal ring gear is used on the outside to constrain the motion of the carrier [13].

Using rigid body kinematics, the output ratio can be found as a function of the tooth counts for a single stage gearbox [14]. Equation (2) gives the effective gear ratio between the carrier and the input sun gear, if the ring gear is held static, and for ratio n, sun gear tooth count n_s and ring gear tooth count n_r.

$$n = \frac{n_s + n_r}{n_r} \tag{2}$$

2.2 LUMPED-PARAMETER THERMAL NETWORK MODELING

Fourier's law of heat transfer, given in Equation (3), governs the flow of heat within a solid body. Complicating matters, however, is the spatial dependence of Fourier's law, such that in many systems its solution is prohibitively difficult to compute in detail [15]. k is the conduction coefficient, T the temperature, $\vec{x}$ the position vector, t the time, and $\dot{q}$ the heat flux.

$$\dot{q}(\vec{x}, t) = -k \nabla T(\vec{x}, t) \tag{3}$$

Newton's law of cooling, seen in Equation (4) meanwhile, is more tractable, but still assumes a temperature gradient within the radiating object, and the convective coefficient used depends on the environmental air speed and geometry and is thus complex to determine [15]. Here $\dot{Q}$ is the total heat flow, h the convection coefficient, A the area, and ΔT the temperature difference.

$$\dot{Q} = hA\Delta T \tag{4}$$

Fundamentally, however, both these laws require modeling the spatial extent of a complex system, and are thus computationally expensive. Instead, when the convective heat transfer from Newton's law of cooling is smaller than the conductive Fourier heat transfer, the conducting elements can be lumped together, and taken as isothermal. Their heat capacities become capacitances, and the conduction and the convection between them resistances. In analogy to electric circuit theory, one then finds Equation (5) and Equation (6) as equivalents to Ohm's law and current conservation, respectively, where ΔT is the temperature difference between two nodes, $\dot{Q}$ the heat flux across an element, and R the thermal resistance [15]. Combining different circuit elements, a thermal network can be constructed for a system akin to an electrical circuit.

$$\Delta T = \dot{Q} R \tag{5}$$

$$\sum \dot{Q} = 0 \tag{6}$$

The regime of validity of this approximation is often considered to be when the dimensionless Biot number Bi is less than 0.1 [5]. The Biot number represents the ratio of

the conductive resistance to convective resistance – if the conduction is faster than the convection, than the conducting object can be treated as an isothermal lumped element [15]. Kircher *et al.*, for instance, numerically calculated the errors of this approximation for a slab with convective heat transfer between two reservoirs, and numerically confirm the $Bi < 0.1$ regime as low in error [16]. Determining the convective heat transfer coefficient h applicable to a gearbox in order to evaluate the Biot number is somewhat complex in the presence of forced convection, and was not attempted. L_c is the characteristic length of the element under consideration, and h and k are as before.

$$Bi = \frac{hL_C}{k} \tag{7}$$

Given a sufficiently low Biot number, a simple thermal network model of a gearbox can be constructed, as seen in Figure 2. Others have previously constructed far more sophisticated models, as described earlier, including detailed component dynamics to estimate the heat generation of individual components [5,6,9,11,17]. Instead, the heat flux will be found experimentally, and the simple model of Figure 3 used. Indeed, with the techniques of circuit theory, a simpler Norton equivalent circuit can be constructed, still with a current source Q_{disp}, but with total capacitance C_{eq} and effective resistance R_{eq} to the ambient (ground) instead of multiple resistors and capacitors. From basic circuit theory, the time constant t_{RC} for such a capacitance-resistor circuit is then given by Equation (8).

$$t_{RC} = C_{eq}R_{eq} \tag{8}$$

The thermal capacitance can be found using Equation (9), where m_{steel} and m_{alum} are the total masses of steel and aluminum, and c_{steel} and c_{alum} are the respective specific heat capacities of steel and aluminum.

$$C_{eq} = m_{steel}c_{steel} + m_{alum}c_{alum} \tag{9}$$

Using this capacitance, the temperature difference between ground and the source, taken as a function of time, can again be found using the results of circuit theory using Equation (10). $T(t)$ is the temperature of the node under consideration at time t, T_i the initial temperature of the steel, and T_f the final asymptotic temperature, $T_f = \lim_{t\to\infty} T(t)$.

$$T(t) = T_i + \left(T_f - T_i\right)e^{-t/t_{RC}} \tag{10}$$

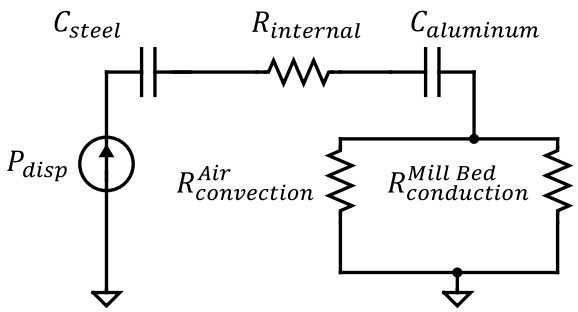

Figure 2: A small thermal network model of the gearbox. The sun, planets, ring gear, and bearings are taken as isothermal, and as a capacitor, C_{steel}, with the heat generating element a current source P_{disp} and situated within the steel components. The aluminum components are likewise considered as a single capacitor, $C_{aluminum}$. There is a thermal resistance internal to the gearbox between the steel and aluminum, $R_{internal}$, as well as convective and conductive resistances between the aluminum and the environment, $R^{Air}_{convection}$ and $R^{Mill\ Bed}_{conduction}$, respectively. It is assumed that the steel is not in thermal contact with the environment, and ambient temperature is taken as the network ground.

Finally, the total dissipated power Q_{disp}, in steady state, can be found as shown in Equation (11), for temperature difference to ambient $\Delta T = \mathrm{T_f} - T_{bed}$, and ground temperature T_{bed}.

$$Q_{disp} = \frac{\Delta T}{R_{eq}} \tag{11}$$

2.3 GEARBOX DISSIPATION MODELS

In addition to the first-principles thermal models described in section 2.2, some prior dissipation versus speed correlations have been published. The American Gear Manufacturers Association (AGMA) promulgates several voluntary standards for gear design, including a set of heat dissipation correlations for enclosed epicyclic gearboxes [1]. Separate correlations are established for load-induced dissipation and no-load dissipation. The latter was found to be principally composed of three elements, shown in Equation (12): the contact seal loss, P_S, the rolling bearing lubricant churning loss, P_{BO}, and the gear churning loss, P_{MO}.

$$P = P_S + P_{BO} + B_{MO} \tag{12}$$

The oil seal loss P_S is found via Equation (13) in terms of a material constant, C_S, shaft diameter D_S, and shaft rotational speed ω_s, in RPM.

$$P_B = C_S D_S \omega_s \quad (13)$$

Likewise, the bearing oil churning P_{BO} is found with Equation (14), for bearing rotational speed ω_B, bearing average diameter d_M, viscosity ν, and a constant C_{BO}.

$$P_{BO} = C_{BO} d_M^3 \nu^{2/3} \omega_B^{5/3} \quad (14)$$

The gear oil churning has many terms, one for each gear, and includes a carrier arrangement constant A_C that AGMA does not specify. It is thus noted here only as a proportionality, in Equation (15), where P_{MO}^i is the loss from an individual gear, R_f a roughness factor, t the gear face width, d the gear pitch diameter, and ω_i the speed of that gear.

$$P_{MO}^i \propto t R_f d^{4.7} \omega_i^3 \quad (15)$$

Due to the constraints of rigid body kinematics, all gear velocities vary linearly with each other up to some constant factor, as in Equation (2), and so for determining functional forms, Equations (13) through (15) may be used without regard for the differences among the input, carrier, and planet gear rotational velocities.

It is worth noting that in addition to gear oil churning, the contact pressure between meshing gear teeth creates high local temperatures in regions of thin lubrication film, sometimes of sufficient magnitude to cause welding of gear material from the surface of one gear to another [18]. This welding phenomenon is known as gear scuffing, and is considered to occur beyond some critical temperature T_{flash}, knowns as the flash temperature. The AGMA 925-A03 standard posits an empirical correlation for this flash temperature for lubricants with extreme pressure additives, given in Equation (16), where ν_{40} is the kinematic viscosity at 40 °C [18].

$$T_{flash} = 118 + 33 \ln \nu_{40} \quad (16)$$

Zhou *et al.* provide a relationship between the heat flux generated by contact pressure between the two gears as a function of gear position within a meshing cycle. While this paper shall not explore the variance of temperature within a single meshing cycle further, Zhou's formula is given in Equation (17) [17]. p is the contact pressure between a pair of gears, β and γ are thermal transfer coefficients, μ_c the coefficient of friction, v_i the pitch-line velocity of the gear, v_j the pitch line velocity of the mating gear, and a_H the semi-contact width, which varies between different meshing angles.

$$P_{mesh} = 2 a_H \beta \mu_c \omega_i \frac{|v_i - v_j|}{v_i} \quad (17)$$

3. GEARBOX THERMAL MEASUREMENT APPARATUS

This case study in gearbox dissipation centered on the particular gearbox designed by MIT Motorsports. A jig was created to fixture and drive this gearbox within a vertical mill, and then instrumentation added in the form of three thermocouples.

3.1 MIT MOTORSPORTS' PLANETARY GEARBOX DESIGN

For the 2021 Formula SAE competition, MIT Motorsports developed a custom epicyclic gearbox, the testing of which is undergone in the foregoing pages. The gearbox constitutes a 6061-aluminum housing and carrier, with a 6.7:1 reduction from the input gear to the output of the carrier, with the gears made from 8620 alloy steel. The carrier rotates between two large diameter sealed thin section bearings. Notably, it is expected that these seals will cause substantive dissipation [3]. The ring gear is assembled into the housing using an interference fit, and likewise, the axles for the planet gears are pressed into the carrier. Both connections are expected to result in excellent thermal contact between the respective components. Finally, the gearbox is filled with a silicon grease for lubrication, specifically Molykote 41® Extreme High Temperature Grease. A computer-aided design (CAD) rendering of this configuration is shown in Figure 3.

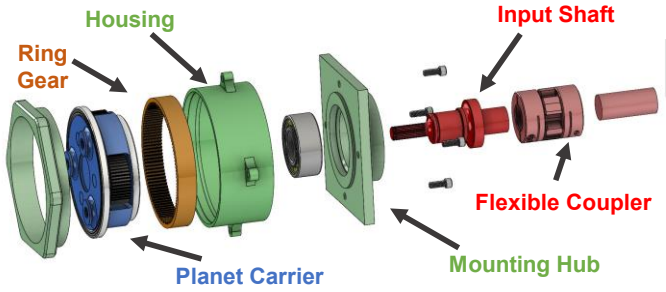

Figure 3: An exploded view of MIT Motorsports' MY21 gearbox design. From left to right, the retaining nut, outboard bearing, ring gear, planet carrier, ring gear, inboard bearing, and housing can be seen. These are all assembled together within the height of the housing, with the aluminum carrier as the output and a separate sun gear in the center (not shown) as the input driving the gearbox.

3.2 TEST JIG AND INSTRUMENTATION

MIT Motorsports' gearbox was mounted within a test jig, in order to constrain it as well as transfer torque from the Haas Mini Mill that was used to drive the gearbox for testing. An aluminum mounting hub was added, with square sides for fixturing, as well as a splined input shaft to adapt to the sun gear. Between the input shaft and the

mill spindle, a flexible coupler was used to avoid added dissipation between the shaft and its bearing due to over constraint. Then, this assembly – show in Figure 4 – was placed into a mill and connected to the spindle, with the mill driving the gearbox during testing.

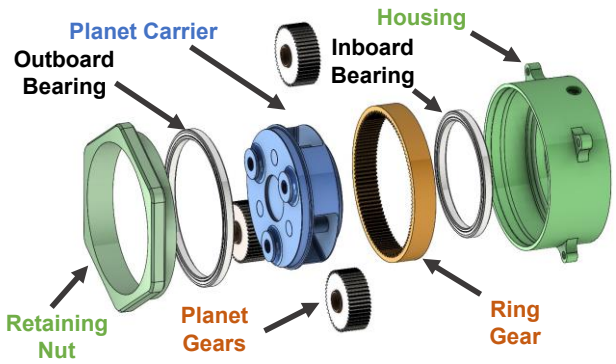

Figure 4: An exploded view of the gearbox testing jig assembly. The housing and mounting hub are both made from 6061 aluminum, while the input shaft, gears, and bearings, are 8620 steel. The system, as taken for the purpose of calculating the thermal capacitance, is assumed to end on the left-hand side at the retaining nut, and on the right-hand side at the splined input shaft.

To measure the temperature within the gearbox, a hole was drilled through the housing and partially into the ring gear to monitor the steel's temperature, as well as a second, shallower hole only into the housing to measure the aluminum's temperature. Vernier TCA-BTA thermocouples were then inserted into these holes, with a third thermocouple bonded to the mill bed to provide a baseline reading. A boron nitride paste was used as a thermal medium between the thermocouples and the measured bodies to ensure low-resistance heat transfer to the probes. Data from the three thermocouples was then collated and time synchronized by a Vernier LabQuest® 3 data acquisition unit, with all samples collected at 5 Hz. Due to equipment limitations, the factory calibrations of the thermocouples were used, with a rated accuracy of ± 3 °C for the temperature ranges measured [19].

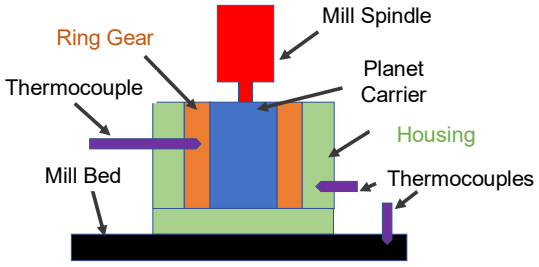

Figure 5: A cartoon diagram of the gearbox test jig. The three thermocouples are shown in purple, with the tip of each purple arrow indicating the depth of penetration. The housing thermocouple only penetrates shallowly into the aluminum, with a depth 3.0 ± 0.1 mm, while the ring gear thermocouple penetrates first through the aluminum, and then partially into the ring gear, with a total depth of 10.9 ± 0.1 mm. The ring gear temperature is assumed to be approximately isothermal with the other gears, since there is excellent convection contact between them via the lubricating grease, and as directly measuring the planet and ring gears is technically unfeasible.

3.3 SYSTEM PARAMETERS FOR THERMAL CAPACITANCE

The thermal network model used invokes an effective equivalent capacitance of the entire system, C_{eq}, in Equation (9). To compute C_{eq}, the mass of each component in the jig was needed, and were thus taken from design data provided by MIT Motorsports, split between 8620 steel and 6061 aluminum components. The specific heat capacities of 8620 and 6061, c_{steel} and $c_{aluminum}$, were also required, and taken as $c_{steel} = 0.475 \frac{\text{J}}{\text{kg°C}}$ and $c_{aluminum} = 0.858 \frac{\text{J}}{\text{kg°C}}$ from published values [20]. The total equivalent thermal capacitance was then found as $C_{eq} = 2{,}659 \frac{\text{J}}{\text{kg°C}}$; since errors were reported on neither the component masses nor the specific heat capacities, no error bounds are reported on this value, and it is instead used as a basis to calibrate the model.

4. RESULTS AND DISCUSSION

The gearbox was run for 25 minutes for each experiment, with spindle speeds between 1000 RPM and 7000 RPM, and the temperature rise of the ring gear, housing, and mill bed monitored using the thermocouples. An exponential curve was fit to the temperature time series generated in order to compute ΔT and t_{RC}, and then using Equations (8) and (10), as well C_{eq} from section 3.3, the dissipated power from each run was determined. Analysis

of the power vs. speed dependence revealed a $\omega^{5/3}$ dependence, as expected for lubricant churning losses from the AGMA model.

4.1 SYSTEM PARAMETERS FOR THERMAL CAPACITANCE

For each run of the gearbox, the collected temperature data was fit to the model function in Equation (10), with uniformly low model parameter errors across all runs' fits, fractionally 0.1%. The data from a representative run is shown in Figure 6, taken at $7000\ RPM$.

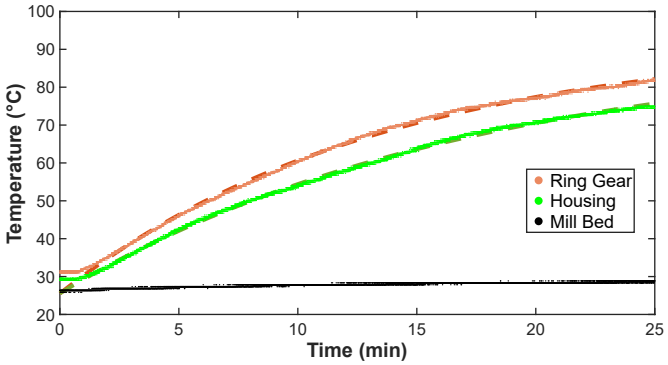

Figure 6: The temperature vs. time series of the gearbox, taken at 7000 RPM. An asymptotic temperature rise can be observed, as evidenced by the fitted exponential function from Equation (10): $T(t) = T_i + (T_f - T_i)e^{-t/t_{RC}}$. For the ring gear, the fitted parameters are $T_i = 25.5 \pm 0.1$ °C, $T_f = 92.7 \pm 0.1$ °C, and $t_{RC} = 13.5 \pm 0.1$ min. Similarly, for the housing, $T_i = 25.5 \pm 0.1$ °C, $T_f = 91.0 \pm 0.2$ °C, and $t_{RC} = 17.2 \pm 0.1$ min.

In terms of the thermal network model, the difference between both the final temperatures T_f and the time constants t_{RC} are expected. Since the steel is closer to the heat source than the aluminum housing, it is expected that it will be at a higher temperature, as seen in the data. Additionally, said difference is small – only 1.7 ± 0.2 °C – justifying the assumption to take the housing and ring gear as isothermal for the simplified lumped mass model. The increased time constant, meanwhile, can be explained as the difference between taking the capacitance of the aluminum and steel in series with the ring gear versus in parallel when measured from the housing, as this results in a higher capacitance, and hence a longer time constant by Equation (8).

4.2 DETERMINATION OF THERMAL RESISTANCE AND TEMPERATURE RISE

Each speed was tested at least twice, and then the fit parameters were plotted in aggregate. The predicted asymptotic temperature rise, $\Delta T = T_f - < T_{bed} >$, for both the ring and the housing is plotted in Figure 7, where T_{bed} is the mean temperature of the mill bed. Likewise, the fitted time constants t_{RC} for the ring gear and housing are shown in Figure 8 at various speeds. Lines are fit to both sets of data, showing consistently increasing ΔT with respect to rotation speed ω, and constant t_{RC} with respect to ω.

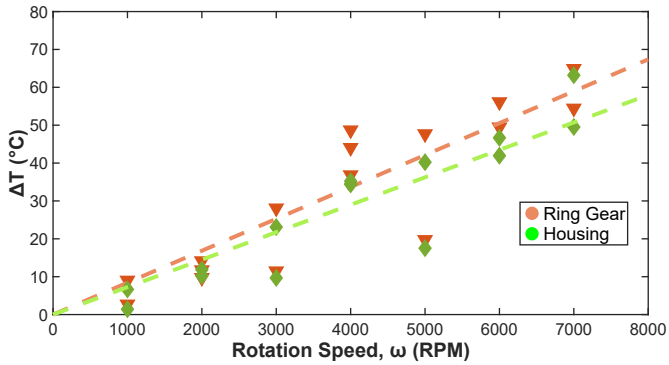

Figure 7: The model final temperature rise, ΔT, from various runs at different speeds. A proportional function, $\Delta T(\omega) = a\omega$ was then fit separately to the ring gear and housing data. For the ring gear, a positive proportionality constant of $a_{steel} = 0.0084 \pm 0.0011$ °C/RPM was found, whereas the aluminum housing had a lower slope of $a_{aluminum} = 0.0072 \pm 0.0010$ °C/RPM. Both fits imply increasing ΔT with rotation speed. Notably, however, the difference between them is not statistically significant: $a_{steel} - a_{aluminum} = 0.0012 \pm 0.0015$ °C/RPM. Confidence intervals for individual datapoints from the fit parameters are smaller than the markers on the plot, and hence not shown.

The temperature rise seen in Figure 7 is both intuitively reasonable, since viscous losses in the lubricant are dependent on fluid velocities, and agrees with existing models. Zhou *et al.*, for instance, note a similar increase between gear bulk temperature and gear velocity, though their result is concave with respect to velocity, indicating there may be effects at higher speeds not evident in these measurements [17]. Paschold et al, meanwhile, also found an increase in bulk temperature with respect to speed, but their result was convex [9]. This experiment does not permit comment on the relative merits of Zhou's vs. Paschold's models, however, since the relation found is fairly coarse, with a 13% error on the model fit parameter.

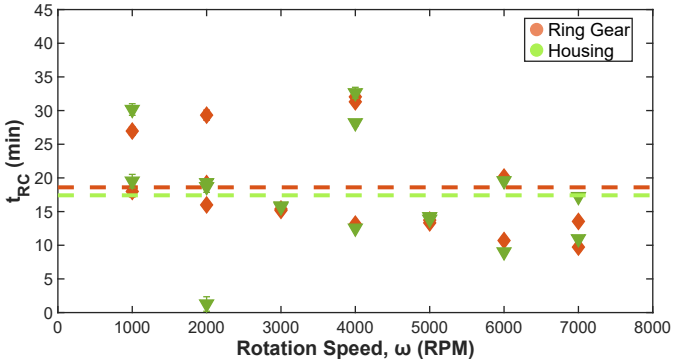

Figure 8: The fitted time constant t_{RC} of the ring gear and the housing temperature data, plotted with respect to operating speed. No statistically significant slope was found for either the ring gear or the housing data sets, implying a constant t_{RC} with respect to ω. A mean value of $t_{RC} = 18.6 \pm 3.8$ min was found for the ring gear data set, and of $t_{RC} = 17.3 \pm 4.0$ min for the housing data sets. As with the temperature data, the difference between the two values is not statistically significant. When larger than the point markers, 95% confidence intervals are shown on individual data points.

The static time constants found in Figure 8 also agrees with the model assumptions – the thermal capacitance should not vary with respect to operating speed or temperature given constant mass, and by Equation (8), since the capacitance is constant, the resistance must be as well. However, the error range on these means is quite high – a fractional uncertainty of 20% for the ring gear – and it is reasonable to suppose substantial variance between samples in the actual cooling rates, be it from external air currents or different fluid conditions. Further work would be needed to discover the true underlying cause of the variance in t_{RC} vales, focused on studying the modes of heat transfer out of the gearbox, both convective and conductive. For the purposes of calculating the dissipation of each sample, however, the resistance can be calibrated using Equation (8) on a per-sample basis, avoiding the complexity of the aforementioned thermal analysis.

4.3 INFERRED DISSIPATION

For each sample run, a t_{RC} and a $\Delta T = T_f - T_i$ were calculated in section 4.2. Using Equation (8), R_{eq} can be found, and then with Equation (11), the P_{disp} computed for each point. Shown in Figure 9 are the results of this calculation for the ring gear, as well as a fit to the gear churning dissipation model from Equation (14). While a similar calculation could be made for the housing, it would require a more complete solution to the thermal network, since the resistances of the aluminum vs. the housing are not distinguished in R_{eq}. Instead, it is assumed all heat is generated either in the steel gears themselves, or the lubricant, and then transferred either to the housing and then ground. Additionally, while other fits were possible with statistically significant coefficients, the $\omega^{5/3}$ dependence used yielded the lowest root-mean-square error, hence its selection here.

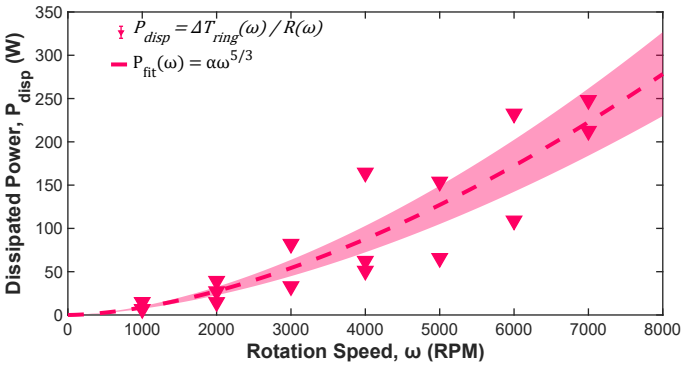

Figure 9: The estimated dissipated power from the ring gear during each sample run. The power from each sample was computed using Equation (11), and then fit to the different AGMA dissipative modes. The best fit was to the gear oil churning model, taken as $P = \alpha\omega^{5/3}$, where $\alpha = (87 \pm 15)\,\frac{\mu W}{RPM^{5/3}}$. Error bars for the data points are not shown, as they are smaller than the plot markers.

The domination of churning losses is somewhat unexpected – the AGMA 925-A03 standard, for instance, suggests gear lubricant churning should only become significant beyond a pitch line velocity of 80 m/s, whereas the maximum velocity tested here is 18 m/s [18]. Conversely, a grease was used for lubrication instead of an oil, and so higher lubrication losses are reasonable. Furthermore, the convex power dissipation found agrees well with the results of Paschold *et al.*, who also note a convex dependence of no-load dissipation on speed [9].

In turn, this suggests that future design work should focus on improving the lubricant performance and selection for a given application. Equation (14) provides a direct relationship between viscosity and the churning losses, indicating lower viscosities should yield less dissipation. However, this is counterbalanced by the need to avoid scuffing. The flash temperature of Equation (16) also varies with viscosity, and will provide a lower bound on acceptable lubricant viscosity. Such a compromise could be ameliorated with better cooling, preventing scuffing while allowing lower viscosities, and whose sizing could be enabled by the dissipation data presented

in Figure 9. Alternatively, since the loaded meshing dissipation found in Equation (17) is a function of relative gear velocity, if possible, lower gear ratios would provide better efficiency, as would lower overall speeds due to the $\omega^{5/3}$ dependence. Such dependencies should be further explored before their use on safety critical systems, and hence a study repeating this dissipation measurement, but sweeping across different lubricants as well, would be valuable.

The model presented here has substantial limitations, however. It neglects the thermal capacity of the lubricant, as well as the difference between the bearings and the gears, both of which are dissipative elements with potentially distinct temperatures. Future work would benefit from distinguishing between the gear and bearing temperature monitoring to allow for better isolation of heat sources. Furthermore, Zhou *et al.*'s modeling of the pressure heating over an individual tooth surface suggests some caution in the use of the isothermal assumption taken herein: Zhou found a local temperature rise of over $80\ °\mathrm{C}$ between points on the tooth surface over the line of contact [17]. The method presented here also requires calibration for each gearbox, and has little numeric predictive powers for alternate geometries. That said, simplicity has a value of its own, as the small number of inputs makes it easier to avoid modeling errors compared to heavily parametrized models.

5. CONCLUSIONS

A thermal testing apparatus for an epicyclic gearbox was constructed and run across a range of speeds. The resulting data was fit to a thermal model, allowing for the estimation of the total dissipated power as $P_{disp} = \alpha\omega^{5/3}$, where $\alpha = (87 \pm 15)\frac{\mu\mathrm{W}}{\mathrm{RPM}^{5/3}}$. This result agrees well with prior work, matching the functional dependence established by the AGMA industry standard for gear churning losses, as well as experiments by others. Additionally, no statistically significant difference was found between the housing and ring gear temperatures rises with respect to speed, and hence the lumped mass assumption of the thermal network model is affirmed as reasonable.

The domination of lubricant losses suggests a focus for future work on the effects of lubricant viscosity, as well as the need to better understand lubricant dynamics during meshing and the consequent heating. Key limitations of the model used include its estimation of the system thermal capacity, a lack of fidelity with regard to dissipative elements, and the requirement for calibration with each gearbox geometry. It nevertheless provides meaningful data, with direct engineering conclusions to lower lubricant viscosity and input speed, if possible.

ACKNOWLEDGMENTS

The author is grateful to the Edgerton Center for access to its testing equipment and tooling, as well to the MIT Motorsports Team for use of its prototypes, funds, and engineering data. Additionally, he is thankful to Dr. Barbara Hughey and Professor Bischofberger for their assistance in planning and implementing the project, as well to Kate Parsons for her thoughtful reviews. Finally, he would like to thank the Pappalardo Machine Shop staff for their generous consultations and advice.

REFERENCES

[1] American Gear Manufacturers Association. *Design Manual for Enclosed Epicyclic Gear Drives*. ANSI/AGMA 6123-C16. Alexandria, Virginia: American Gear Manufacturers Association, approved August 16th, 2016, reaffirmed October 2021.

[2] Liu, P., and Feng, S., 2020, "Integrated Motor and Two-Speed Gearbox Powertrain System Development for Electric Vehicle," *12th Annual IEEE Energy Conversion Congress and Exposition, ECCE 2020, October 11, 2020 - October 15, 2020*, Institute of Electrical and Electronics Engineers Inc., Virtual, Detroit, MI, United states, pp. 1499–1504.

[3] Gnauert, J., Schluter, F., Jacobs, G., Bosse, D., and Witter, S., 2021, "Simulative Investigation of Ring Creep on a Planetary Bearing of a Wind Turbine Gearbox," Forschung im Ingenieurwesen/Engineering Research, **85**(2), pp. 219–227.

[4] Boris, Ryan, 2020. Manager, Geartrain Engineering, Tesla, private communication.

[5] Sivayogan, G., Rahmani, R., and Rahnejat, H., 2020, "Lubricated Loaded Tooth Contact Analysis and Non-Newtonian Thermoelastohydrodynamics of High-Performance Spur Gear Transmission Systems," Lubricants, **8**(2), p. 20 (26 pp.).

[6] Wang, J., Liu, N., Wang, H., and E, J., 2021, "Analysis of Nonlinear Dynamic Characteristic of a Planetary Gear System Considering Tooth Surface Friction," Proceedings of the Institution of Mechanical Engineers, Part J: Journal of Engineering Tribology, **235**(11), pp. 2376–2395.

[7] Neurouth, A., Changenet, C., Ville, F., and Octrue, M., 2017, "Influence of Rolling Element Bearing Modeling on the Predicted Thermal Behavior of the FZG Test Rig," Tribology Transactions, **60**(4), pp. 753–761.

[8] Brousek, J., and Zvolsky, T., 2018, "Experimental Study of Electric Vehicle Gearbox Efficiency," *BulTrans-2018 - 10th International Scientific Conference on Aeronautics, Automotive and Railway Engineering and Technologies, 15-17 Sept. 2018*, EDP Sciences, France, p. 02004 (5 pp.).

[9] Paschold, C., Sedlmair, M., Lohner, T., and Stahl, K., 2021, “Calculating Component Temperatures in Gearboxes for Transient Operation Conditions,” Forsch Ingenieurwes.

[10] Changenet, C., Oviedo-Marlot, X., and Velex, P., 2006, “Power Loss Predictions in Geared Transmissions Using Thermal Networks-Applications to a Six-Speed Manual Gearbox,” Journal of Mechanical Design, Transactions of the ASME, **128**(3), pp. 618–625.

[11] Chen, L. F., Wu, X. L., Qin, D. T., and Wen, Z. J., 2011, “Thermal Network Model for Temperature Prediction in Planetary Gear Trains,” Applied Mechanics and Materials, **86**, pp. 415–418.

[12] Corley, B., Carroll, J., and Mcdonald, A., 2020, “Fault Detection of Wind Turbine Gearbox Using Thermal Network Modelling and SCADA Data,” *The Science of Making Torque from Wind (TORQUE 2020), 28 Sept.-2 Oct. 2020*, IOP Publishing, UK, p. 022042 (10 pp.).

[13] 2017, “What Is Epicyclic Gearbox - Main Components, Working and Application?,” Mechanical Booster.

[14] Budynas, R. G., and Nisbett, J. K., 2016, *Shigley’s Mechanical Engineering Design*, McGraw Hill Education.

[15] Cravalho, E., Smith, J., Brisson, J., and McKinley, G., 2005, *Thermal Fluids Engineering, An Integrated Approach to Thermodynamics, Heat Transfer, and Fluid Mechanics*, Oxford University Press.

[16] Kircher, K. J., and Max Zhang, K., 2015, “On the Lumped Capacitance Approximation Accuracy in RC Network Building Models,” Energy and Buildings, **108**, pp. 454–62.

[17] Zhou, C., Xing, M., Wang, H., and Hu, B., 2021, “A Novel Thermal Network Model for Predicting the Contact Temperature of Spur Gears,” International Journal of Thermal Sciences, **161**, p. 106703.

[18] American Gear Manufacturers Association. *Effect of Lubrication on Gear Surface Distress*. ANSI/AGMA 925-A03. Alexandria, Virginia: American Gear Manufacturers Association, approved August 16th, 2016, reaffirmed October 2021.

[19] “Thermocouple User Manual – Vernier” [Online]. Available: https://www.vernier.com/manuals/tca-bta/. [Accessed: 17-Apr-2022].

[20] Rice, R., Jackson, J., Bakuckas, J., and Thompson, S., 2003, “Metallic Materials Properties Development and Standardization (MMPDS-01).”